Myocardin regulates BMP10 expression and is required for heart development

Jianhe Huang,[1,2] John Elicker,[1,2] Nina Bowens,[1,3] Xi Liu,[1] Lan Cheng,[1] Thomas P. Cappola,[1,2] Xiaohong Zhu,[1] and Michael S. Parmacek[1,2]

[1]University of Pennsylvania Cardiovascular Institute, [2]Department of Medicine, and [3]Department of Surgery, University of Pennsylvania, Philadelphia, Pennsylvania, USA.

Myocardin is a muscle lineage–restricted transcriptional coactivator that has been shown to transduce extracellular signals to the nucleus required for SMC differentiation. We now report the discovery of a myocardin/BMP10 (where BMP10 indicates bone morphogenetic protein 10) signaling pathway required for cardiac growth, chamber maturation, and embryonic survival. Myocardin-null (Myocd) embryos and embryos harboring a cardiomyocyte-restricted mutation in the *Myocd* gene exhibited myocardial hypoplasia, defective atrial and ventricular chamber maturation, heart failure, and embryonic lethality. Cardiac hypoplasia was caused by decreased cardiomyocyte proliferation accompanied by a dramatic increase in programmed cell death. Defective chamber maturation and the block in cardiomyocyte proliferation were caused in part by a block in BMP10 signaling. Myocardin transactivated the *Bmp10* gene via binding of a serum response factor–myocardin protein complex to a nonconsensus CArG element in the *Bmp10* promoter. Expression of $p57^{kip2}$, a BMP10-regulated cyclin-dependent kinase inhibitor, was induced in $Myocd^{-/-}$ hearts, while BMP10-activated cardiogenic transcription factors, including NKX2.5 and MEF2c, were repressed. Remarkably, when embryonic $Myocd^{-/-}$ hearts were cultured ex vivo in BMP10-conditioned medium, the defects in cardiomyocyte proliferation and $p57^{kip2}$ expression were rescued. Taken together, these data identify a heretofore undescribed myocardin/BMP10 signaling pathway that regulates cardiomyocyte proliferation and apoptosis in the embryonic heart.

Introduction

In vertebrates, the heart is the first organ to form and its function is required for diffusion of nutrients to the embryo and removal of waste (1). Formation of the embryonic heart is a complex process involving a series of sequential morphogenetic events, including cardiogenic induction, cardiomyocyte differentiation and proliferation, specification of noncardiomyocyte lineages, formation and patterning of the primitive heart tube, looping morphogenesis, and finally, chamber maturation (2). These events are governed by an ancient developmental program involving the interplay of cardiogenic transcription factors and growth factors secreted from cardiomyocytes and nonmyocytic cell lineages. Mutations in the genes encoding these cardiogenic transcription factors and growth factors are associated with common forms of congenital heart disease (3, 4).

Cardiogenic transcription factors lie at the core of the developmental pathways regulating specification of cardiogenic precursors and morphogenesis of the heart (1, 5, 6). Serum response factor (SRF) is a MADS (MCM1, AGAMOUS, DEFICIENS, SRF) box transcription factor that is enriched in mesodermal lineages (7). Conditional ablation of the *Srf* gene in the embryonic mouse heart leads to embryonic lethality attributable to cardiac insufficiency during chamber maturation (8–10). Our group and others have shown that the cardiomyocyte- and SMC-restricted transcriptional coactivator myocardin physically associates with SRF and synergistically activates transcription of a subset of CArG (CC(A/T)6GG) box–containing genes (11). Expression of myocardin is first observed in the cardiac crescent, and subsequently, it is expressed throughout the embryonic myocardium and postnatal heart (12). In addition, myocardin is expressed abundantly in vascular and visceral SMCs. Myocardin-null ($Myocd^{-/-}$) embryos survive through E10.5, which has been attributed to a block in vascular SMC differentiation (13). Ablation of the *Myocd* gene in neural crest–derived vascular SMCs revealed that myocardin promotes the contractile vascular SMC phenotype (14). In contrast, much less is understood about the function of myocardin in the embryonic and adult heart. In *Xenopus laevis*, morpholino-directed knockdown of myocardin mRNA results in inhibition of cardiac development and the absence of expression of cardiac differentiation markers with disruption of cardiac morphological processes (15). Ablation of the *Myocd* gene in the adult mouse heart leads to the rapid onset of dilated cardiomyopathy and heart failure (16). However, the molecular basis of myocardin function in the embryonic and adult heart remains unclear.

Members of the bone morphogenetic protein (BMP) family of secreted growth factors regulate multiple steps in the cardiogenic program (17, 18). Bmp10, a cardiac-restricted BMP family member, plays a critical role in regulating development of the heart (19, 20). Bmp10 is first expressed in the mouse heart at embryonic day E8.75 and subsequently becomes enriched within the trabecular myocardium between E9.0 and E13.5: a developmental window devoted to cardiac growth and chamber maturation (20). $Bmp10^{-/-}$ embryos survive through E10.5, but succumb from heart failure associated with a normally patterned, but severely hypoplastic, heart (20). Transgenic mice that overexpress Bmp10 during postnatal development demonstrate a 50% reduction in cardiac size (21). Interestingly, a substitution variant of BMP10, Thr326Ile, was identified in patients with hypertensive dilated cardiomyopathy (22). However, it is not clear what mechanisms regulate expression of BMP10 during embryonic or postnatal development.

In this report, we generated and characterized myocardin-null and conditional mutant mice in which the *Myocd* gene was selec-

Conflict of interest: The authors have declared that no conflict of interest exists.
Citation for this article: *J Clin Invest.* 2012;122(10):3678–3691. doi:10.1172/JCI63635.

Table 1
Genotype distribution of offspring generated from intercrossing *Myocd*$^{+/-}$ mice

Age	*Myocd*$^{+/+}$ (WT)	*Myocd*$^{+/-}$ (Het)	*Myocd*$^{-/-}$ (Null)
E8.5	49 (24.6%)	99 (50.0%)	51 (25.4%)
E9.0	23 (25.8%)	45 (50.5%)	21 (23.7%)
E9.5	125 (26.9%)	249 (53.5%)	91 (19.6%)
E10.5	24 (33.8%)	47 (66.2%)	0 (0%)

tively ablated in cardiomyocytes. *Myocd*$^{-/-}$ embryos survive until E9.5–E10.0 and exhibit severe defects in cardiac morphogenesis and function. Selective ablation of the *Myocd* gene in the embryonic heart (*Nkx2-5Cre*$^{+}$*Myocd*$^{F/F}$) recapitulates many of the defects observed in *Myocd*$^{-/-}$ embryos, with embryonic lethality observed at E13.5. Myocardial hypoplasia is attributable to a decrease in cardiomyocyte proliferation accompanied by a dramatic increase in cardiomyocyte apoptosis. Surprisingly, the observed defects in cardiac structure and function are attributable, at least in part, to myocardin-induced activation of the *Bmp10* gene. Bmp10, in turn, regulates expression of several cardiogenic transcription factors, including Nkx-2.5 and Mef2c and the cyclin-dependent kinase inhibitor p57^{kip2}. Remarkably, when grown ex vivo, defects in cardiomyocyte proliferation in the hearts of E9.5 *Myocd*$^{-/-}$ embryos are rescued in the presence of Bmp10-conditioned medium. These data demonstrate that myocardin lies upstream of Bmp10 signaling in a cardiogenic program regulating cardiac growth, chamber maturation, and ultimately, embryonic survival.

Results

Myocd$^{-/-}$ *embryos develop hypoplastic hearts and a block in chamber maturation*. *Myocd*$^{-/-}$ mice were generated by selectively deleting exon 8 of the *Myocd* gene (Supplemental Figure 1, A–D; supplemental material available online with this article; doi:10.1172/JCI63635DS1). This gene-targeting strategy differs from that described in an earlier report resulting in deletion of *Myocd* exons 8 and 9 (13). Genotype analysis of 824 embryos harvested from staged *Myocd*$^{+/-}$ × *Myocd*$^{+/-}$ intercrosses revealed that *Myocd*$^{-/-}$ embryos survive until E9.5–E10.0 (Table 1). In situ hybridization analyses performed with a myocardin antisense riboprobe confirmed that myocardin mRNA is expressed abundantly throughout the embryonic heart (Figure 1A). In contrast, myocardin mRNA was markedly attenuated in hearts of E8.5–E9.5 *Myocd*$^{-/-}$ embryos (Figure 1B). At E9.5 and E10.0, *Myocd*$^{-/-}$ embryos were readily identifiable by their size, which was consistently smaller than that of WT and heterozygote control littermates (Figure 1, C and D). By E10.5, *Myocd*$^{-/-}$ embryos were not viable and were undergoing various states of reabsorption. Moreover, at or before E10.0, all viable *Myocd*$^{-/-}$mutant embryos displayed pericardial effusions indicative of heart failure (Figure 1D).

Inspection of hearts harvested from E10.0 *Myocd*$^{-/-}$ mutant embryos revealed that these hearts had undergone rightward looping with the future left ventricle directed toward the left side of the pericardial cavity and the bulbus-cordis region located on the right side of the pericardial cavity (Figure 1, E–H). 3D high resolution optical mapping of E9.5 control and mutant embryos immunostained with MLC2v antibody to identify cardiac myocytes confirmed that the hearts of *Myocd*$^{-/-}$ embryos have completed looping morphogenesis (Supplemental Videos 1 and 2). In addition, scanning EM of E9.5 WT and *Myocd*$^{-/-}$ hearts confirmed that looping morphogenesis had occurred in the *Myocd*$^{-/-}$ hearts (Figure 1, I and K). However, sections cut through the ventricle of E9.5 *Myocd*$^{-/-}$ embryos revealed gross defects in cardiac growth and chamber maturation characterized by thinning of the ventricular myocardium (Figure 1, J and L) and a block in trabeculation (Figure 1, J and L, and Figure 2, T and X). In E9.5 WT embryos, the ventricular compact zone is composed of 3–5 layers of cardiomyocytes, and the process of trabecular invagination has begun (Figure 1J). In contrast, in *Myocd*$^{-/-}$ hearts, the compact zone is composed of 1–2 layers of cardiomyocytes, and trabeculation is rarely observed (Figure 1L).

Myocd$^{-/-}$ *hearts exhibit morphogenetic defects prior to differentiation of vascular SMCs*. Histological analyses of hearts of control and *Myocd*$^{-/-}$ embryos revealed subtle differences in development of the compact zone myocardium as early as E8.75 (Figure 2, A–H). In control embryos, the compact zone consisted of 3–5 layers of tightly packed cardiomyocytes (Figure 2, A–D). In contrast, the compact zone of *Myocd*$^{-/-}$ hearts consisted of only 1–3 layers of irregularly spaced cardiomyocytes (Figure 2, E–H). Between E9.0 and E9.5, the loss of compact zone cellularity in *Myocd*$^{-/-}$ embryos became even more pronounced (Figure 2, I–X). In addition, the trabecular myocardium was severely attenuated or absent in the mutant embryos (Figure 2, M–P and U–X). Marked changes in development of the atrioventricular canal (AVC) were also observed in E9.0–E9.5 *Myocd*$^{-/-}$ embryos (Figure 2, I–X). At E9.0, expansion of the truncus arteriosus region of outflow tract (OFT) and AVC was readily observed in control embryos (Figure 2, I–L). In contrast, the OFT and AVC were underdeveloped in *Myocd*$^{-/-}$ hearts (Figure 2, M–P). Of note, the observed decrease in myocardial cellularity in the hearts of E8.75–E9.0 *Myocd*$^{-/-}$ embryos occurred prior to changes attributable to a block in vascular SMC differentiation (23).

Myocd$^{-/-}$ *embryos develop heart failure*. To examine cardiac function in *Myocd*$^{-/-}$ embryos, echocardiography was performed in utero on a series of E9.5 control and *Myocd*$^{-/-}$ embryos. Telemetric ECG recordings revealed severe bradycardia, which is often associated with heart failure during embryonic development, in *Myocd*$^{-/-}$ embryos compared with WT littermates (63 ± 8 beats/minute in *Myocd*$^{-/-}$ embryos [n = 10] versus 139 ± 11 beats/minute in WT littermates [n = 12]; $P < 0.0001$). In WT control embryos, synchronous atrial and ventricular cardiac contractions were readily identified (Supplemental Videos 3 and 4). However, in E9.5 *Myocd*$^{-/-}$ embryos, a marked decrease in systolic function was observed (Supplemental Videos 5 and 6). In some planes of section, a small pericardial effusion was also apparent (Supplemental Video 5). Comparison of systolic to diastolic ventricular dimensions, or fractional shortening, in 6 E9.5 controls and 6 *Myocd*$^{-/-}$ embryos revealed a decrease from 37.3% ± 3.5% in control embryos to 18.5% ± 2.3% in *Myocd*$^{-/-}$ embryos ($P < 0.01$). Taken together, these data demonstrate that heart failure contributed to the embryonic demise of *Myocd*$^{-/-}$ embryos.

Myocardial hypoplasia results from decreased cardiomyocyte proliferation and increased cardiomyocyte apoptosis. To determine whether the myocardial hypoplasia observed in *Myocd*$^{-/-}$ hearts resulted from a decrease in cardiomyocyte proliferation and/or an increase in apoptosis, hearts harvested from E8.5–E9.5 control and *Myocd*$^{-/-}$ embryos were immunostained for markers of cell proliferation and apoptosis. At E9.5, a period of rapid expansion of the compact and trabecular zones (6), WT hearts demonstrated robust cardiomyocyte proliferation. Expression of phospho-histone H3 (pHH3),

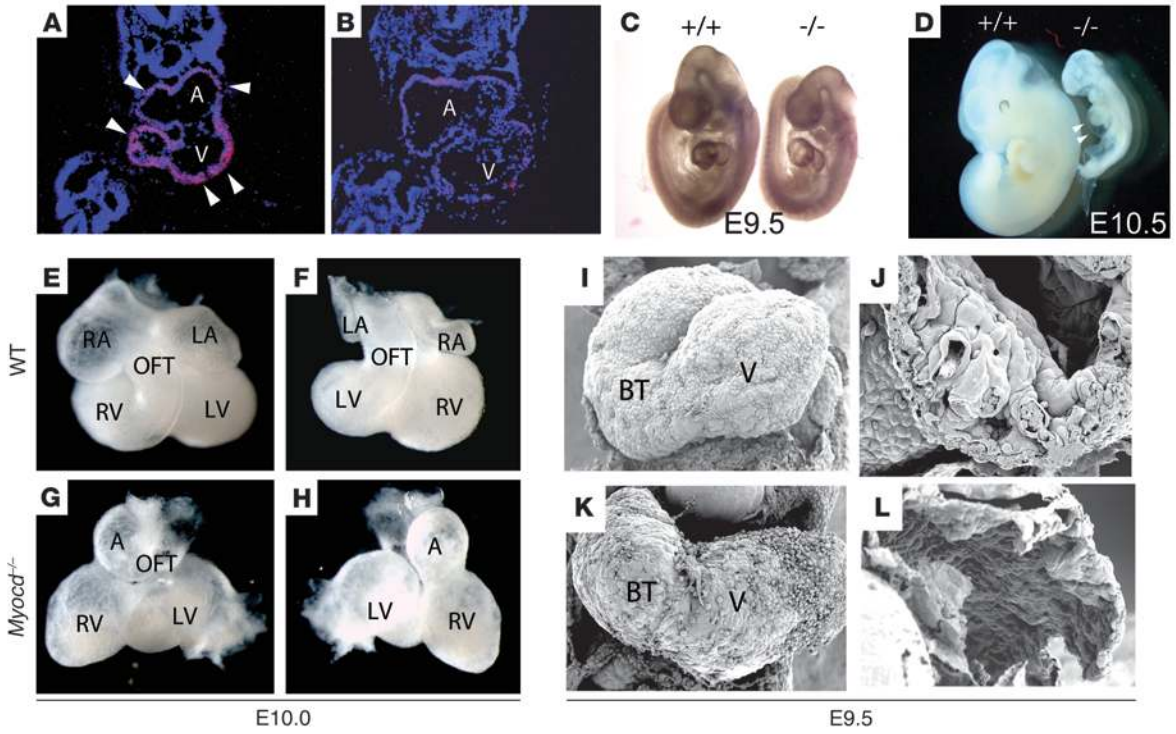

Figure 1

Myocd$^{-/-}$ embryos exhibit hypoplastic hearts and heart failure. (**A** and **B**) In situ hybridization analysis performed with radiolabeled antisense myocardin riboprobe to sections prepared from E9.5 control (**A**) and *Myocd*$^{-/-}$ (**B**) embryos demonstrating myocardin mRNA (arrowheads, pink signal) throughout the common atria (A) and ventricle (V) of control mice, but only background levels in *Myocd*$^{-/-}$ hearts. Original magnification, ×40. (**C** and **D**) Whole-mount preparation of E9.5 (**C**) and E10.5 (**D**) WT (+/+) and *Myocd*$^{-/-}$ (–/–) mutant mice. E10.5 mutants exhibit growth retardation and pericardial effusion (arrowheads) indicative of heart failure. (**E**–**H**) Hearts harvested from E10.0 WT (**E** and **F**) and *Myocd*$^{-/-}$ mutant (**G** and **H**) embryos shown from frontal (**E** and **G**) and dorsal (**F** and **H**) perspective, demonstrating that both the WT and mutant hearts have completed the stage of looping morphogenesis. The future right and left atria (RA, LA), right ventricle, left ventricle, and OFT are identified. (**I**–**L**) Scanning electron micrographs of hearts harvested from E9.5 WT (**I** and **J**) and *Myocd*$^{-/-}$ mutant (**K** and **L**) embryos, demonstrating that the *Myocd*$^{-/-}$ mutant ventricle (**L**) is hypoplastic and underdeveloped compared with the WT heart (**J**). Original magnification, ×200 (**I** and **K**); ×500 (**J** and **L**). See also Supplemental Figure 1 and Supplemental Videos 1–6.

which correlates with mitotic chromosomal condensation, was observed in 24.0% of cardiomyocytes compared with only 9.6% of cardiomyocytes in *Myocd*$^{-/-}$ hearts (Figure 3, A–C) ($P < 0.01$). Proliferating cell nuclear antigen (PCNA) was observed in 68% of cardiomyocytes in WT hearts compared with 13% of cardiomyocytes in mutant hearts (Figure 3, D–F) ($P < 0.01$). Expression of the G_1/S-specific cyclin, cyclin D2, was observed in 55% of cardiomyocytes in WT hearts, but only 18.8% of mutant cardiomyocytes (Figure 3, G–I) ($P < 0.01$). BrdU, which was injected into pregnant dams 2 hours prior to embryo harvest, was incorporated in 12.5% of cardiomyocytes in WT hearts compared with 2.5% of cardiomyocytes in the mutant hearts (Figure 3, J–L) ($P < 0.01$). Taken together, these data demonstrate a marked decrease in embryonic cardiomyocyte proliferation in E9.5 *Myocd*$^{-/-}$ mutant hearts.

TUNEL staining of hearts harvested from E8.5–E9.5 WT and *Myocd*$^{-/-}$ mutant embryos revealed a marked increase in cardiomyocyte apoptosis in *Myocd*$^{-/-}$ mutant embryos compared with WT littermates (Figure 3, M–O). As early as E8.5, a 3-fold increase in cardiomyocyte apoptosis was observed in the mutant hearts (3.2% ± 0.6% versus 1.0% ± 0.2%; $P < 0.01$). Remarkably, at E9.0, a 12-fold induction in cardiomyocyte apoptosis was observed in *Myocd*$^{-/-}$ mutant hearts compared with WT hearts (12.6% ± 2.2% versus 1.0% ± 0.1%; $P < 0.01$). Similarly, at E9.5, a 13-fold induction in cardiomyocyte apoptosis was observed in *Myocd*$^{-/-}$ hearts compared with WT hearts (13.3% ± 3.5% versus 1.0% ± 0.1%; $P < 0.01$). Electron microscopic analyses revealed ultrastructural changes indicative of widespread cardiomyocyte apoptosis in E9.5 *Myocd*$^{-/-}$ hearts, including nuclear chromatin aggregation and fragmentation and cytoplasmic apoptotic body formation (compare Figure 3, P and Q). In addition, swelling of the mitochondria with breakdown of the mitochondrial membranes was observed in *Myocd*$^{-/-}$ hearts (compare Figure 3, R and S). These analyses demonstrate that myocardial hypoplasia in *Myocd*$^{-/-}$ embryos is attributable to both a decrease in cardiomyocyte proliferation and a dramatic increase in cardiomyocyte apoptosis and that these changes begin at least as early as looping of the primitive heart tube and accelerate during expansion of the compact zone and initiation of trabecularization.

Cardiomyocyte-restricted ablation of the Myocd gene. To determine whether the cardiac phenotype observed in *Myocd*$^{-/-}$ embryos was attributable to the cell-autonomous loss of myocardin function in cardiac myocytes, *Nkx2-5Cre*$^{+}$*Myocd*$^{F/F}$ conditional mutant mice were generated and characterized as harboring a cardiomyocyte-restricted mutation in the *Myocd* gene. Of note, the Nkx2-5 pro-

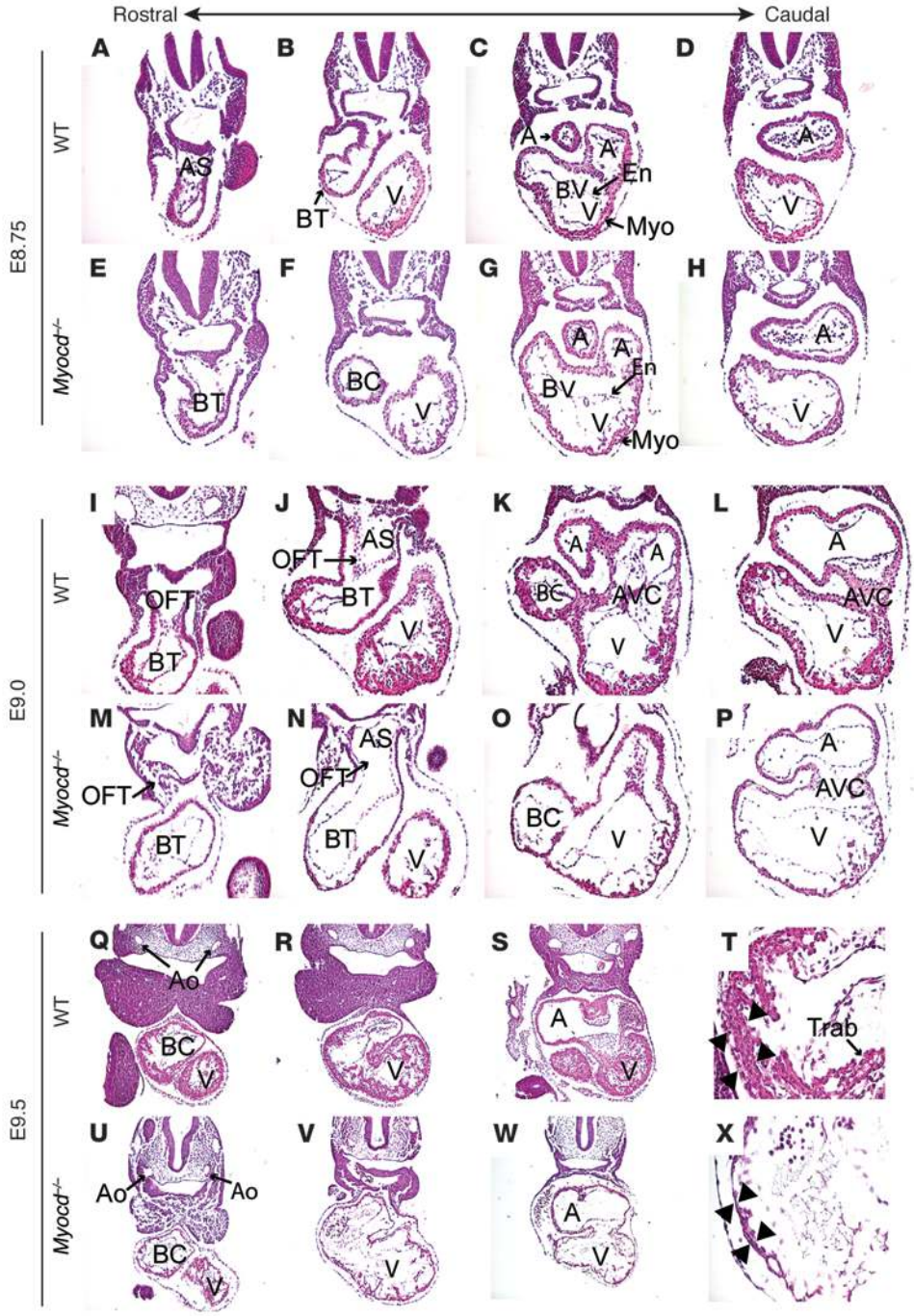

Figure 2

Myocd$^{-/-}$ mutant embryos develop a block in chamber maturation. (**A**–**H**) H&E-stained sections of E8.75 WT (**A**–**D**) and *Myocd*$^{-/-}$ (**E**–**H**) embryos demonstrating initiation of looping morphogenesis with identifiable common atria, common ventricle, bulbus-cordis (BC), bulbus-ventricular region (BV), bulbus-truncus (BT), and aortic sac (AS). A single endocardial (EN) layer is observed at this stage of development. The compact zone of the WT ventricle (**C** and **D**) is composed of 4–6 layers of densely packed cardiac myocytes (Myo), while the compact zone of *Myocd*$^{-/-}$ hearts is composed of 1–3 layers of cardiac myocytes. Original magnification, ×200. (**I**–**P**) At E9.0, the AVC and cardiac OFT are well developed in WT hearts (**I**–**L**). In *Myocd*$^{-/-}$ hearts, the AVC and OFT are wide open and cardiac jelly in these regions is substantially decreased (**M**–**P**). In addition, in *Myocd*$^{-/-}$ hearts, the compact and trabecular zones of the primitive ventricle are thinned, disorganized, and markedly underdeveloped. Original magnification, ×200. (**Q**–**X**) At E9.5, control (**Q**–**T**) and *Myocd*$^{-/-}$ mutants (**U**–**X**) have completed looping morphogenesis and normally undergo chamber maturation. The paired dorsal aortas (arrowheads, Ao) are seen in control and mutant embryos at this stage of development. Compared with control hearts, the compact zone of *Myocd*$^{-/-}$ mutant hearts is hypocellular (arrowheads) and disorganized, and there is a block in development of trabecular (Trab) myocardium. Original magnification, ×100 (**Q**–**S** and **U**–**W**); ×400 (**T** and **X**).

moter was utilized in these experiments because Nkx2-5Cre–mediated recombination was observed at E7.5 throughout the cardiac crescent, thereby elucidating the function of myocardin during the earliest stages of cardiogenesis (24). Genotype analysis of E8.5–P21 littermates generated from intercrosses of *Nkx2-5Cre*$^{+}$*Myocd*$^{F/+}$ mice revealed that *Nkx2-5Cre*$^{+}$*Myocd*$^{F/F}$ mutant mice survive until E13.5–E14.5 (Table 2). E13.5 *Nkx2-5Cre*$^{+}$*Myocd*$^{F/F}$ mutant embryos demonstrated signs of heart failure, including generalized edema and large pericardial effusions (Figure 4, A and B). As anticipated, in E12.5 *Nkx2-5Cre*$^{+}$*Myocd*$^{F/F}$ hearts, myocardin mRNA was markedly attenuated (compare Figure 4, E and F). Quantitative RT-PCR (qRT-PCR) performed with cardiac mRNA harvested from E12.5 control and conditional mutant embryos revealed a 90% decrease in expression of myocardin mRNA in the conditional mutant hearts. In contrast, comparable levels of myocardin mRNA were observed in visceral SMCs populating the trachea and esophagus of control and mutant embryos (Figure 4, E and F). Consistent with these observations, nuclear expression of myocardin was reduced dramatically in *Nkx2-5Cre*$^{+}$*Myocd*$^{F/F}$ mutant hearts compared with control hearts (Figure 4, G and H). Breeding of the *Myocd* conditional mutant mice into a Rosa26 genetic background confirmed that WT (*Nkx2-5Cre*$^{+}$*Myocd*$^{F/+}$*Rosa26*$^{+}$) and myocardin-deficient (*Nkx2-5Cre*$^{+}$*Myocd*$^{F/F}$*Rosa26*$^{+}$) cardiomyocytes are indeed derived from Nkx-2.5–expressing cardiomyocytes and/or progeni-

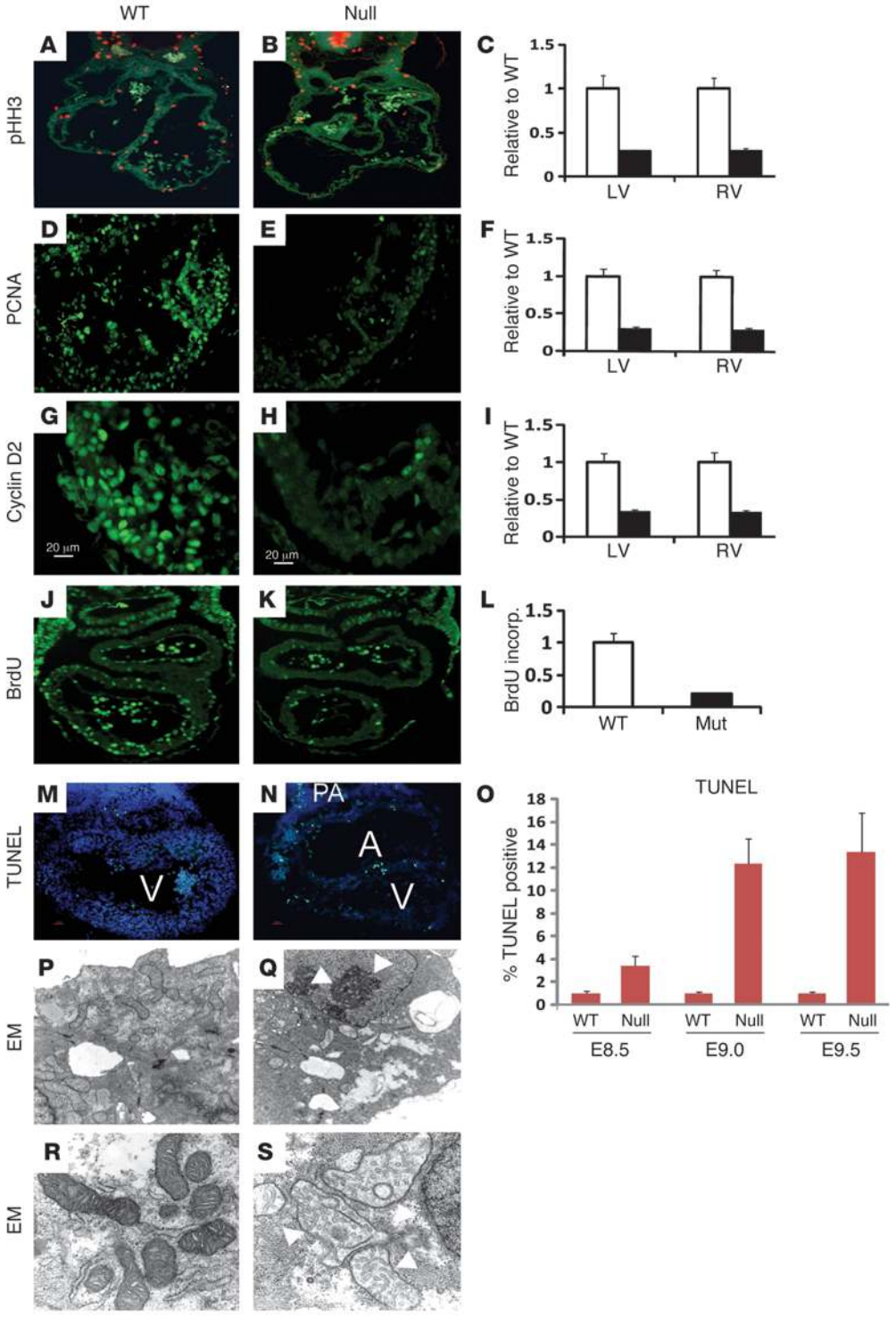

Figure 3

Myocd$^{-/-}$ hearts exhibit decreased cardiomyocyte proliferation and increased apoptosis. (**A**–**L**) Assessment of cardiomyocyte proliferation in hearts of E9.5 WT and *Myocd*$^{-/-}$ (null) embryos. Histological sections showing hearts of E9.5 WT and *Myocd*$^{-/-}$ (null) embryos were immunostained with antibodies that recognize pHH3 Ser10 (**A**–**C**; orange stain), PCNA (**D**–**F**; green stain), cyclin D2 (**G**–**I**; green stain), and BrdU (**J**–**L**; green stain). White bars represent WT and black bars represent *Myocd*$^{-/-}$ embryos. Immunostained cardiomyocytes in the bulbus-cordis (RV) and future left ventricle (LV) were quantified by a blinded observer, and data are expressed as mean number of immunostained ventricular cardiomyocytes per high power field in *Myocd*$^{-/-}$ hearts compared with WT hearts ± SEM ($P < 0.01$, control versus mutant for each marker). (**M**–**O**) Analysis of apoptosis in E8.5–E9.5 control (WT) and *Myocd*$^{-/-}$ mutant (null) hearts by TUNEL staining. (**M**–**O**) Sections of E.8.5, E9.0, and E9.5 WT and *Myocd*$^{-/-}$ (null) embryos were immunostained for TUNEL activity (green) and costained with DAPI (blue). TUNEL-positive cardiomyocytes per high power field were quantified by a blinded observer, and data are expressed as mean percentage of TUNEL-positive cardiomyocytes ± SEM ($P < 0.01$, control versus mutant for each marker). (**P**–**S**) EM of E9.5 WT and *Myocd*$^{-/-}$ mutant hearts revealed nuclear chromatin aggregation, nuclear fragmentation, and cytoplasmic apoptotic body formation (Figure 2Q, arrowheads) in hearts of *Myocd*$^{-/-}$ embryos. Mitochondrial swelling with breakdown of the mitochondrial membranes was also observed in *Myocd*$^{-/-}$ hearts (Figure 2S, arrowheads). Original magnification, ×50,000.

tor cells (Figure 4, C and D). Taken together, these data demonstrate that the phenotype observed in *Nkx2-5Cre*$^{+}$*Myocd*$^{F/F}$ conditional mutant embryos is attributable to cardiomyocyte-restricted loss-of-function of myocardin.

Consistent with the phenotype of *Myocd*$^{-/-}$ mutant embryos, the hearts of E13.5–E14.5 *Nkx2-5Cre*$^{+}$*Myocd*$^{F/F}$ conditional mutant embryos demonstrated severe myocardial hypoplasia (Figure 4, I–L). In E13.5 *Nkx2-5Cre*$^{+}$*Myocd*$^{F/F}$ embryos, the ventricular compact zone consisted of only 1–4 layers of irregularly spaced cardiomyocytes versus 5–10 layers of densely packed cardiomyocytes in control littermates (Figure 4, K and L). In *Nkx2-5Cre*$^{+}$*Myocd*$^{F/F}$ embryos, a large ventricular septal defect (VSD) that is not normally observed at this stage of development was routinely observed (Figure 4, I and J). However, defects in aortic and mitral valve formation were not observed in E13.5 *Nkx2-5Cre*$^{+}$*Myocd*$^{F/F}$ embryos (Figure 4, I and J, and data not shown). Once again, a

Table 2
Genotype distribution of offspring generated from intercrossing *Nkx2.5Cre+/MyocdF/+* mice with *MyocdF/F* mice

Age	*Nkx2.5Cre+/MyocdF/F*	*Nkx2.5Cre+/MyocdF/+*	*MyocdF/F*	*MyocdF/+*
P21	0 (0%)	26 (33.7%)	25 (32.4%)	26 (33.7%)
E16.5	0 (0%)	43 (33.3%)	42 (32.6%)	44 (34.1%)
E15.5	1 (1.4%)	24 (32.4%)	25 (33.8%)	24 (32.4%)
E14.5	3 (3.7%)	25 (30.9%)	26 (32.1%)	27 (33.3%)
E13.5	18 (10.7%)	49 (29.2%)	51 (30.4%)	50 (29.8%)
E12.5	40 (19.8%)	53 (26.2%)	54 (26.7%)	55 (27.2%)
E11.5	28 (24.8%)	28 (24.8%)	29 (25.7%)	28 (24.8%)
E10.5	18 (24.7%)	17 (23.2%)	19 (26.0%)	19 (26.0%)

significant decrease in cardiomyocyte proliferation was observed in E13.5 conditional mutant embryos (Figure 4, M–O). 46% ± 6% of cardiomyocytes in control hearts incorporated BrdU versus 26% ± 3.3% in the conditional mutant hearts ($P < 0.01$). Even more remarkable was the 11-fold increase in the cardiomyocyte apoptosis in E12.5 *Nkx2-5Cre+Myocd F/F* hearts compared with control littermates (Figure 4, P–R). The apoptotic index observed in conditional mutant hearts was 11.7% ± 1.1% versus 1.0% + 0.1% in control hearts ($P < 0.01$). These data demonstrate that ablation of the *Myocd* gene in embryonic cardiomyocytes (or progenitor cells) causes a block in cardiac growth and chamber maturation associated with decreased cardiomyocyte proliferation and a marked increase in cardiomyocyte apoptosis.

Myocardin-regulated genes and the fetal cardiac program. To examine the molecular basis of myocardin function in the embryonic heart, qRT-PCR was performed with mRNA harvested from E9.0 WT and *Myocd*$^{-/-}$ hearts and primers that amplify genes involved in the cardiogenic program (Figure 5A). As anticipated, myocardin mRNA was expressed abundantly in control hearts, but was undetectable in *Myocd*$^{-/-}$ hearts (Figure 5A). The closely related transcriptional coactivators Mrtf-A/Mkl1 and Mrtf-B/Mkl2 were also expressed at comparable levels in control and *Myocd*$^{-/-}$ hearts. In addition, the *Gata-4* and *Srf* genes were expressed at comparable levels in control and *Myocd*$^{-/-}$ hearts (Figure 5A). In contrast, *Nkx-2.5*, *Mef2c*, and *Tbx5* gene expression were markedly attenuated in the hearts of *Myocd*$^{-/-}$embryos compared with WT controls. These data suggested that Bmp10, which regulates *Nkx2.5*, *Mef2c*, and *Tbx5* gene expression in the embryonic heart, but not *Gata4* or *Srf* gene expression, may also be regulated (directly or indirectly) by myocardin in the embryonic heart. Indeed, qRT-PCR confirmed that *Bmp10* mRNA was severely attenuated in the hearts of *Myocd*$^{-/-}$ embryos compared with WT embryos (Figure 5A).

Immunostaining of sections prepared from E9.5 control and *Myocd*$^{-/-}$ embryos confirmed that expression of the cardiogenic transcription factors Nkx2.5, Mef2c, and Tbx5 is indeed reduced in the hearts of *Myocd*$^{-/-}$ embryos compared with controls (Figure 5B). In contrast, Gata4 and Srf were expressed at comparable levels in the hearts of *Myocd*$^{-/-}$ and control embryos (Figure 5B). This observation was perplexing, as *Nkx2-5*$^{-/-}$ and *Mef2c*$^{-/-}$ embryos exhibited defects in looping morphogenesis, while *Myocd*$^{-/-}$ and *Nkx2-5Cre+Myocd F/F* embryos did not (25–27). This suggested that expression of Nkx-2.5 and/or Mef2c may be differentially regulated by myocardin (directly or indirectly) during different stages of heart development in the embryo. Consistent with this hypothesis, Nkx-2.5 and Mef2c were expressed abundantly throughout the hearts of E8.5 WT and *Myocd*$^{-/-}$ embryos (Supplemental Figure 2). Interestingly, Nkx2-5 and Mef2c were also developmentally downregulated in hearts of *Nkx2-5Cre+Myocd F/F* conditional mutant embryos, but decreased expression of these factors was delayed by approximately 12 to 24 hours compared with *Myocd*$^{-/-}$ embryos (Supplemental Figure 2). Of note, the temporal alteration in expression of Nkx2-5 and Mef2c once again recapitulated changes observed in hearts of *Bmp10*$^{-/-}$ embryos (20).

The fetal heart program coordinates expression of a unique set of cardiac-, skeletal-, and smooth muscle–restricted genes encoding myofibrillar isoforms (28). Despite significant alterations in several key cardiogenic transcription factors in *Myocd*$^{-/-}$ mutant embryos, comparable levels of myosin heavy chain (MF20), myosin light chain 2V (MLC2v), and cardiac troponin T (cTnT) were observed in the hearts of E8.5–E9.5 WT and *Myocd*$^{-/-}$ embryos (Figure 5B). An important component of the fetal heart program is a subset of SRF/CArG box–dependent genes associated with the SMC contractile phenotype, including SM α-actin (SMA) and SM22α (29). In this regard, it is noteworthy that neither of these genes was expressed in the dorsal aorta of E9.5 *Myocd*$^{-/-}$ mutants (13). This led us to speculate that the observed changes in cardiac structure and function may relate to a block in SRF-regulated genes that compose the fetal heart program. However, comparable levels of SMA and SM22α were observed in the hearts of *Myocd*$^{-/-}$ and control littermates (Figure 5B). These data demonstrate that distinct mechanisms have evolved to regulate expression of SRF-regulated genes that are coexpressed in vascular SMCs and the embryonic heart.

Myocardin regulates Bmp10 and its downstream target genes in the embryonic heart. The timing of embryonic lethality, block in cardiac chamber maturation, and loss of the *Bmp10* gene and target gene expression in *Myocd*$^{-/-}$ embryos suggested strongly that the transcriptional coactivator myocardin lies upstream and regulates Bmp10 signaling in the embryonic heart. Consistent with this observation, immunostaining and quantitative immunoblot analysis revealed a 90% decrease in Bmp10 protein in E9.5 *Myocd*$^{-/-}$ hearts compared with control hearts (Figure 6, A–E). BMP signaling is transduced to the nucleus via activation of Smads 1, 5, and 8 by MAPK and GSK3 (30). Remarkably, immunostaining of E9.5 control and *Myocd*$^{-/-}$ hearts with an antibody that recognizes phosphorylated (activated) Smad1/5/8 demonstrated a dramatic reduction in Smad1/5/8 signaling in the hearts of *Myocd*$^{-/-}$ embryos compared with controls, suggesting generalized repression of BMP signaling in *Myocd*$^{-/-}$ hearts (Figure 6, F–I).

It is also noteworthy that Bmp10 has been shown to suppress the expression and activity of p57^{kip2}, a negative regulator of the cell cycle, which could explain, at least in part, the block in cardiomyocyte proliferation observed in *Myocd*$^{-/-}$ hearts (20). Consistent with this hypothesis, expression of p57^{kip2} was induced in the ventricular compact zone and trabecular myocardium and OFT of E9.0 *Myocd*$^{-/-}$ embryos compared with WT embryos (Figure 6, J–M). Quantitative analyses of p57^{kip2} antibody–stained sections demonstrated greater than a 2-fold increase in p57^{kip2}-positive nuclei in the hearts of *Myocd*$^{-/-}$ embryos compared with control embryos ($P < 0.01$). Taken together, these data demonstrate a block in BMP signaling in myocardin-null hearts manifested as (a) downregulation in *Bmp10* gene expression, (b) downregulation of phosphorylated

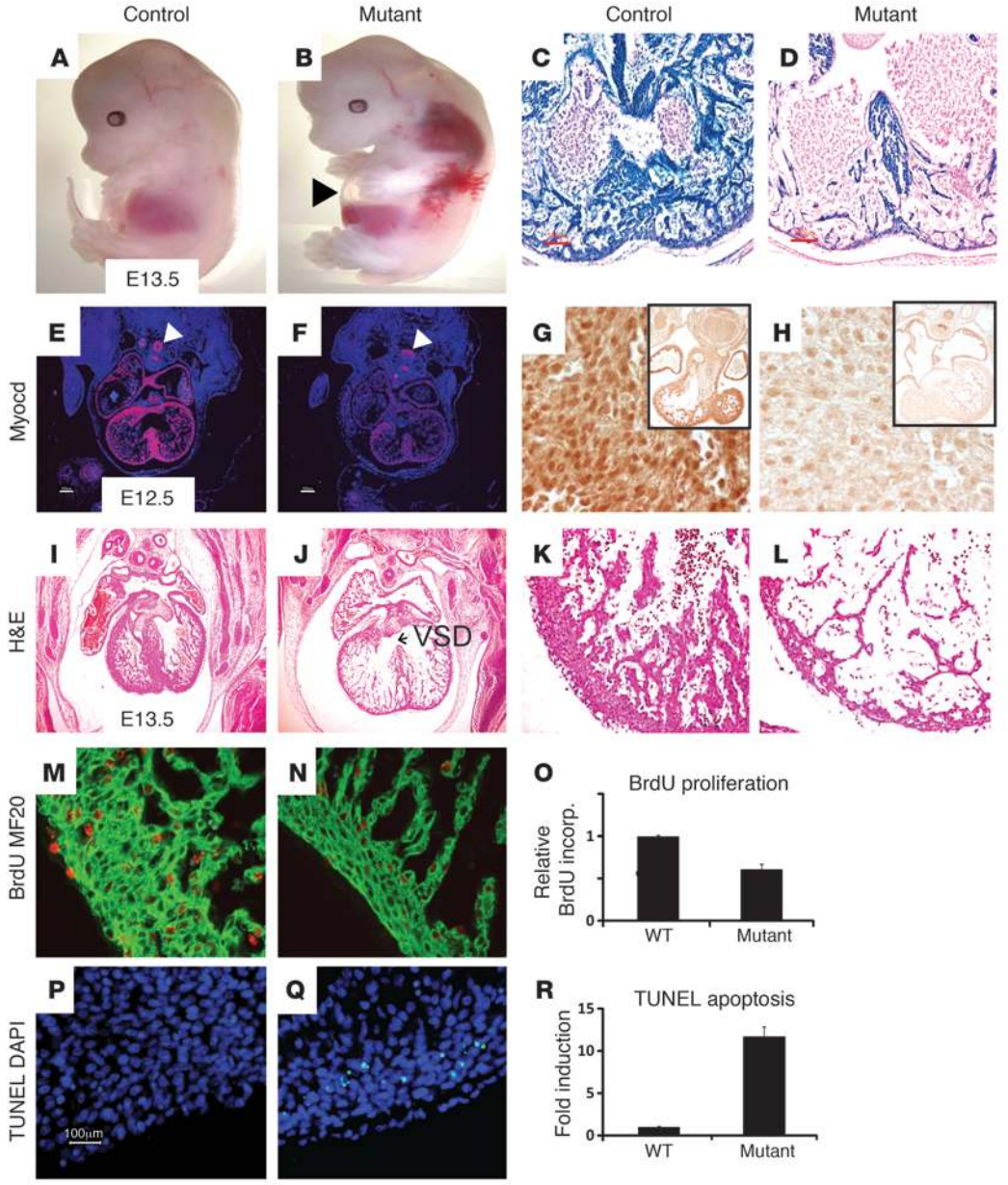

Figure 4

Nkx2-5Cre^{+}*/Myocd*$^{F/F}$ mutant embryos develop hypoplastic hearts attributable to a block in cell proliferation and increased apoptosis. (**A** and **B**) E13.5 *Nkx2-5Cre*$^{+}$*/Myocd*$^{F/F}$ mutant embryo (**B**) exhibits generalized edema and pericardial effusions (arrowhead) compared with *Myocd*$^{F/F}$ control embryo (**A**). (**C** and **D**) E10.5 control *Nkx2-5Cre*$^{+}$*/Myocd*$^{F/+}$*/Rosa26* (**C**) and *Nkx2-5Cre*$^{+}$*Myocd*$^{F/F}$*/Rosa 26* embryos (**D**) demonstrating intense blue staining (LacZ) throughout the myocardium; scale bars: 100 μm. (**E** and **F**) In situ hybridization analyses demonstrating myocardin mRNA (pink signal) throughout control hearts (**E**) and background levels in mutant hearts (**F**). Comparable myocardin is observed in the trachea and esophagus (arrowheads). Original magnification, ×40. (**G** and **H**) E12.5 *Myocd*$^{F/F}$ control (**G**) and *Nkx2-5Cre*$^{+}$*/Myocd*$^{F/F}$ mutant (**H**) embryos demonstrating nuclear expression of myocardin (dark brown stain) in control hearts (**G**) and attenuated expression in mutant hearts. Inset panel shows low-power magnification of heart and surrounding tissues. Original magnification, ×400; ×40 (inset). (**I**–**L**) E13.5 *Myocd*$^{F/F}$ control (**I** and **K**) and *Nkx2-5Cre*$^{+}$*/Myocd*$^{F/F}$ mutant (**J** and **L**) embryos demonstrating thinning of the compact zone and trabecular myocardium and VSD (arrow) in the mutant hearts. Original magnification, ×40 (**I** and **J**); ×200 (**K** and **L**). (**M**–**O**) E13.5 control (**M**) and conditional mutant (**N**) embryos immunostained for BrdU (orange) and MF20 (green) expression. Data expressed as relative number of BrdU-expressing cardiomyocytes in the mutant heart compared with the WT heart ± SEM ($P < 0.01$, control versus mutant). Original magnification, ×400. (**P**–**R**) Apoptosis quantified in E12.5 control (**P**) and *Nkx2-5Cre*$^{+}$*/Myocd*$^{F/F}$ (**Q**) hearts by TUNEL (green stain). Data are expressed as fold induction in TUNEL-positive cardiomyocytes per high power field in mutant compared with control hearts ± SEM ($P < 0.01$). Original magnification, ×200.

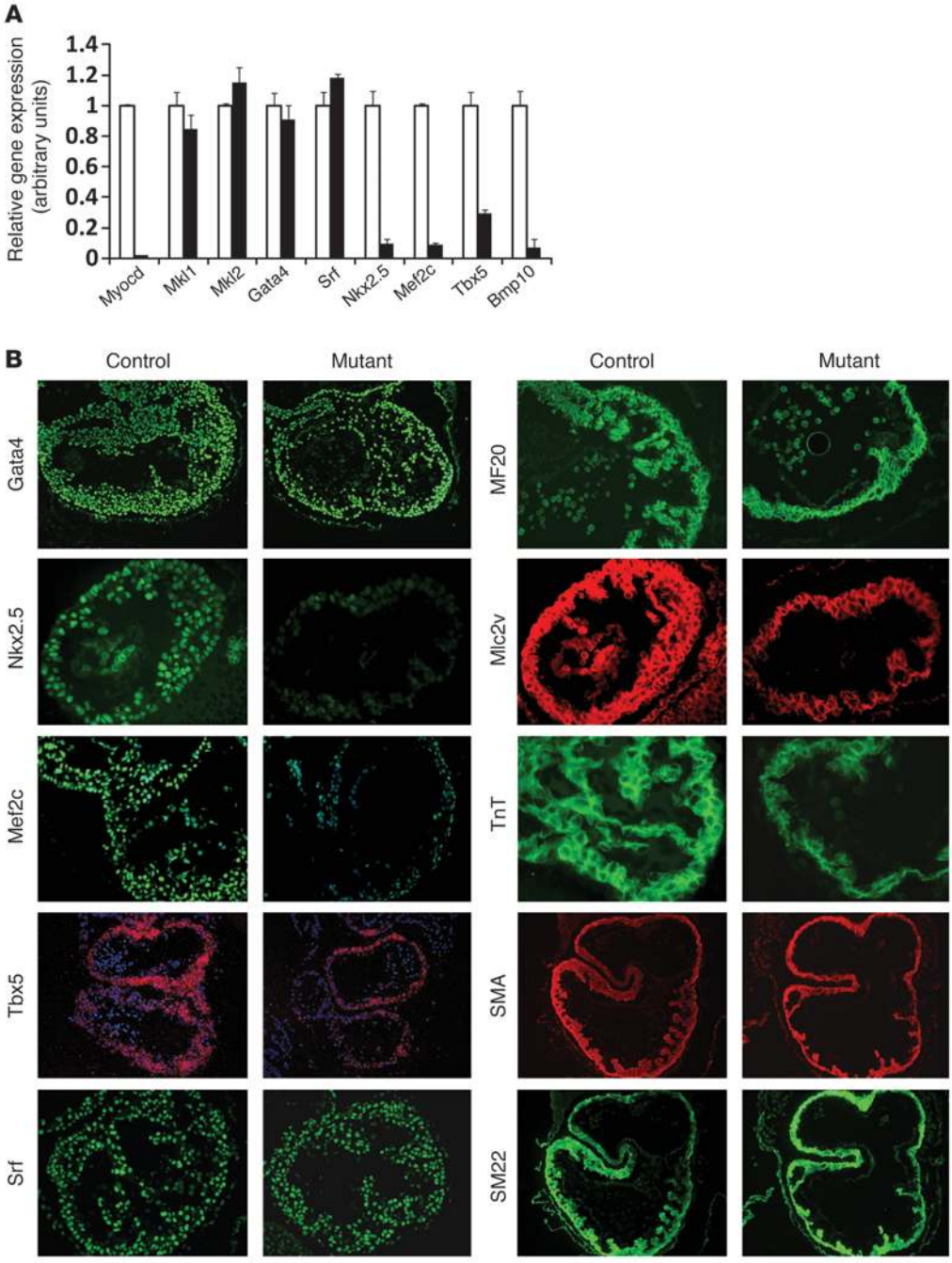

Figure 5
Myocardin regulates expression of key cardiogenic transcription factors and Bmp10 coincident with ventricular chamber maturation. (**A**) qRT-PCR was performed with mRNA harvested from the hearts of 3 E9.5 WT control and 3 *Myocd*$^{-/-}$ mutant embryos as described in Methods. White bars (controls) and black bars (mutants) show the relative level (arbitrary units) of *Myocd*, *Mkl1*, *Mkl2*, *Gata4*, *Srf*, *Nkx-2.5*, *Mef2c*, *Tbx5*, and *Bmp10* gene expression. Data are expressed as relative gene expression in mutant compared with WT control hearts (arbitrary units) ± SEM. (**B**) Immunohistochemical analyses of markers of cardiomyocyte differentiation in E9.5 WT control and *Myocd*$^{-/-}$ (mutant) hearts. Sections were immunostained with antibodies that recognize Gata4, Nkx-2.5, Mef2c, Srf, myosin heavy chain (MF20) (green stain), Mlc2v (red stain), cardiac troponin T (cTnT) (green stain), SMA (red stain), and SM22α (SM22). In situ hybridization analysis performed with radiolabeled antisense Tbx5 riboprobe (red signal) to sections prepared from E9.5 control and *Myocd*$^{-/-}$ embryos. See also Supplemental Figure 2.

Smad1/5/8 signaling, (c) downregulation of the Bmp10-regulated cardiogenic transcription factors Nkx2.5 and Mef2c, and finally, (d) increased expression of the cell cycle inhibitor p57^{kip2}.

The Bmp10 promoter is activated directly by myocardin. As schematically depicted in Figure 7A, a search of GenBank with the TRANSFAC database revealed that the mouse *Bmp10* promoter contains a near consensus (9 of 10 nucleotide identity) SRF-binding site, or CArG motif, at position –515 to –524. In addition, a second near-consensus CArG box (CCTAAACTGG) is located at bp –1163 in the mouse *Bmp10* promoter. Near-consensus CArG boxes, each containing a 1-bp substitution mutation in the central $(AT)_6$ nucleotide sequence, were also identified in the rat, human, and chicken *BMP10* promoters (Figure 7A). EMSA performed with nuclear extracts prepared from Cos7 cells transfected with an expression plasmid encoding the 935–amino acid cardiac-restricted isoform of myocardin or SRF revealed a low-mobility nuclear protein complex that bound specifically to the nonconsensus CArG box motif in the *Bmp10* promoter (Figure 7B, lanes 1–5 and 9). This nuclear protein complex was markedly attenuated when increasing amounts of unlabeled nonconsensus CArG box oligonucleotides were added to the incubation reaction (Figure 7B, lanes 6, 7). Moreover, addition of SRF antibody to the binding reaction super-shifted this nuclear protein complex, demonstrating that this nuclear protein complex contains Srf or an antigenically related protein (Figure 7B, lanes 8

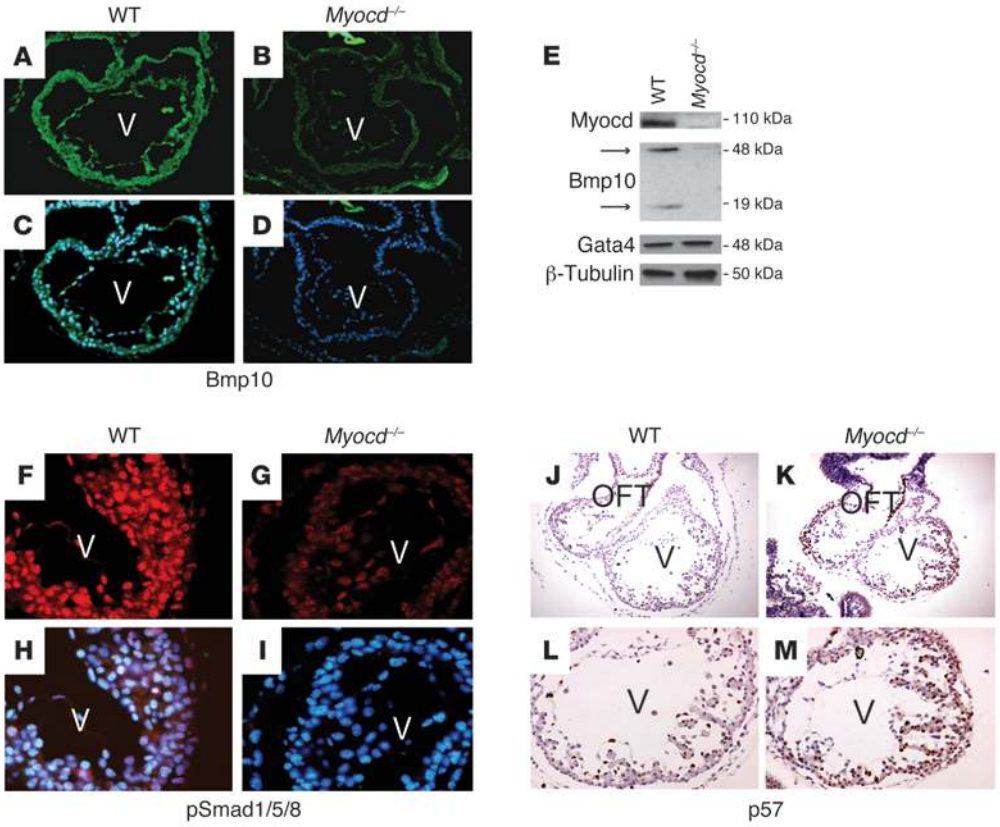

Figure 6

Myocardin regulates Bmp10 signaling and $p57^{kip2}$ expression in the embryonic heart. (**A**–**D**) Sections of E9.0 WT (**A** and **C**) and *Myocd*$^{-/-}$ (**B** and **D**) mutant hearts were immunostained with anti-Bmp10 antibody (green stain) and counterstained with DAPI (**C** and **D**; blue stain). Bmp10 immunostaining is markedly reduced in *Myocd*$^{-/-}$ hearts compared with control hearts. (**E**) Immunoblot analysis of protein lysates prepared from the hearts of E9.5 WT and *Myocd*$^{-/-}$ embryos. Blots were hybridized to Myocd, Bmp10, Gata4, and β-tubulin antibodies, respectively. Arrows denote pro-BMP and processed Bmp10 protein, respectively. Quantitative analysis of the hybridization signal (normalized to β-tubulin) revealed a 90% decrease in Bmp10 expression in *Myocd*$^{-/-}$ hearts compared with controls. MW markers are shown to the right of each blot. See also Supplemental Uncut gels. (**F**–**I**) Sections of E9.5 WT (**F** and **H**) and *Myocd*$^{-/-}$ (**G** and **I**) hearts were immunostained with anti-pSmad1/5/8 antibody and counterstained with DAPI (**H** and **I**). pSmad1/5/8 expression is markedly reduced in *Myocd*$^{-/-}$ hearts compared with WT hearts. (**J**–**M**) Sections of E9.0 WT (**J** and **L**) and *Myocd*$^{-/-}$ (**K** and **M**) hearts were immunostained with anti-$p57^{kip2}$ antibody and costained with eosin. $p57^{kip2}$ expression is markedly increased in the compact and trabecular zone myocardium of *Myocd*$^{-/-}$ hearts compared with WT hearts.

and 10). Similarly EMSAs performed with the nonconsensus CArG box motif in the human *BMP10* promoter demonstrated specific binding of a myocardin-SRF protein complex to the human *BMP10* promoter (data not shown).

To determine whether this CArG motif is required for transcriptional activity of the 795-bp mouse *Bmp10* promoter, a series of transient cotransfection analyses were performed. Cotransfection of Cos7 cells with the pcDNA.MyocdL expression plasmid, encoding the 935–amino acid isoform of myocardin, and the pBmp10.luc reporter plasmid demonstrated a 38-fold increase in luciferase activity compared with cells cotransfected with the pcDNA3 control plasmid and pBmp10.luc (Figure 7C, lanes 2 and 5). Similarly, cotransfection with the pcDNA.MyocdS expression plasmid, encoding the 856-amino acid smooth muscle–restricted isoform of myocardin, which binds Srf, but not Mef2c (31), and pBmp10.luc resulted in a 35-fold increase in luciferase activity compared with cells cotransfected with pcDNA3 and pBmp10.luc (Figure 7C, lanes 2 and 6). In contrast, cotransfection of Cos7 cells with the pμBmp10.luc reporter plasmid, which contains the *Bmp10* promoter with a mutation that abolishes binding of SRF/myocardin to the embedded CArG motif (Figure 7A), and pcDNA.MyocdL or pcDNA.MyocdS, respectively, failed to increase luciferase activity above levels observed in cells cotransfected with pcDNA3 and to pBmp10.luc or pμBMP10.luc, respectively (Figure 7C, lanes 2, 7, and 8).

In addition, ChIP assays performed with crosslinked DNA harvested from E9.5 hearts confirmed that an SRF-myocardin complex binds to the nonconsensus CArG element in the mouse *Bmp10* promoter in vivo. As anticipated, when chromatin was immunoprecipitated with an anti-SRF antibody and the input DNA amplified with primers flanking the consensus CArG box in the *c-fos* promoter, 18-fold enrichment of the input DNA was observed (Figure 7D). Similarly, when the crosslinked cardiac chromatin was amplified with PCR primers flanking the nonconsensus CArG box in the mouse *Bmp10* promoter, 28-fold enrichment of the input DNA was observed (Figure 7D). Moreover, 20-fold enrichment was observed when crosslinked cardiac chromatin was immunoprecipitated with anti-myocardin antibody and DNA was amplified with primers flanking the CArG box in the *Bmp10* promoter (Figure 7D). Taken together, these data demonstrate that a nuclear protein complex containing myocardin and Srf binds to a nonconsensus and conserved CArG box in the *Bmp10* promoter transactivating the *Bmp10* gene.

Bmp10 rescues the defect in cell proliferation in Myocd$^{-/-}$ *hearts.* These findings suggested a model wherein myocardin activates transcription and expression of BMP10, which in turn suppresses $p57^{kip2}$ expression, thereby inducing cardiomyocyte proliferation in the embryonic heart. To test this hypothesis, NIH3T3 cells were stably transduced with control lentivirus encoding EGFP or with a lentivirus encoding mouse Bmp10, generating control and Bmp10-conditioned medium, respectively. Immunoblot analysis confirmed that stably transduced NIH3T3 cells secreted abundant Bmp10

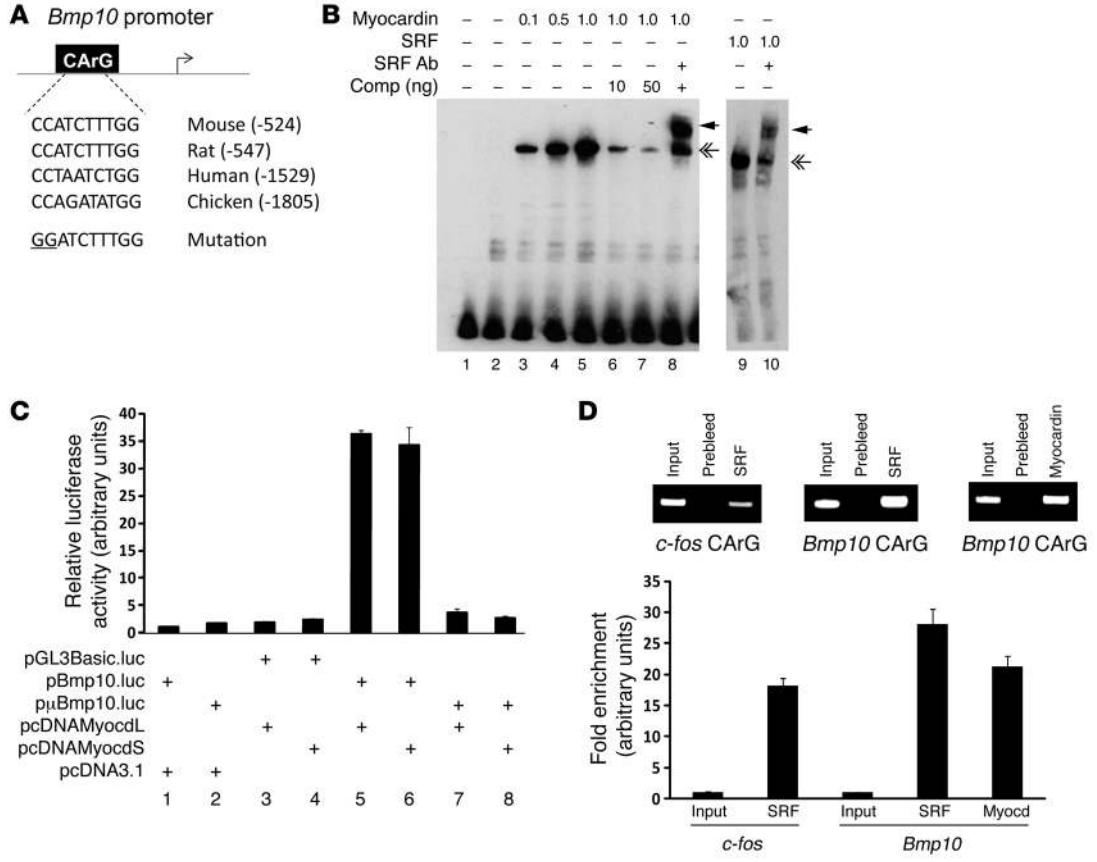

Figure 7

Myocardin binds to and transactivates the *Bmp10* promoter. (**A**) Schematic representation of the *Bmp10* promoter and CArG boxes identified (genomic location) in the mouse, rat, human, and chicken *BMP10* promoters, respectively. The nucleotide sequence of the mutant CArG box utilized in EMSA and transient transfection analyses is shown below. (**B**) EMSAs performed with biotin-labeled mouse *Bmp10* CArG box oligonucleotide and nuclear extracts prepared from Cos7 cells transfected with an expression plasmid-encoding myocardin, SRF, or pcDNA3. Where indicated, binding reaction mixtures included unlabeled competitor oligonucleotide or anti-SRF antibody. The low-mobility nuclear protein complex containing SRF and myocardin is indicated with a double arrow to the right, and the supershifted complex is denoted by a single arrow. (**C**) Transient transfection analysis of Cos7 cells cotransfected with pcDNA.MyocdL or the pcDNA.MyocdS expression plasmid and the indicated luciferase reporter plasmid. Luciferase activity is reported as mean luciferase activity compared with luciferase activity in cells cotransfected with the pcDNA3 plasmid ± SEM. (**D**) ChIP assays performed with chromatin harvested from the hearts of E9.5 embryos. Chromatin was immunoprecipitated with anti-SRF antibody, anti-myocardin antibody, or preimmune rabbit sera (negative control). qRT-PCR was performed with PCR primers flanking either the mouse *c-fos* promoter CArG box or the mouse *Bmp10* promoter CArG box. The upper panels show amplified DNA products immunoprecipitated with either anti-SRF antibody or anti-myocardin antibody. The graph shows qPCR quantification of amplified DNA expressed as fold-enrichment (arbitrary units) normalized to input DNA ± SEM.

(data not shown). To determine whether Bmp10-conditioned medium rescues the defect in cell proliferation observed in *Myocd*$^{-/-}$ mutant hearts, hearts were isolated from E9.5 WT control and *Myocd*$^{-/-}$ embryos and grown ex vivo for 48 hours in the presence of Bmp10-conditioned medium ($n = 5$) or control conditioned medium ($n = 5$). As anticipated, WT hearts were significantly larger than *Myocd*$^{-/-}$ hearts and consistently beat more rapidly and vigorously over the course of 48 hours in culture (Supplemental Videos 7–10 and Figure 8, A–F). In control hearts, following 24 hours of incubation with BrdU, 88.2% ± 0.6% of cardiac myocytes incorporated BrdU (Figure 8G). In contrast, only 56.1% ± 0.9% of ventricular cardiomyocytes incorporated BrdU in *Myocd*$^{-/-}$ hearts (Figure 8H) ($P < 0.01$ versus control hearts). However, when grown in the presence of Bmp10-conditioned medium, 85.2% ± 0.7% of ventricular cardiomyocytes in *Myocd*$^{-/-}$ hearts incorporated BrdU (Figure 8I) ($P < 0.001$ versus control medium). Consistent with these findings, 22.7% ± 0.3% of ventricular cardiomyocytes expressed the cell proliferation marker pHH3 (Figure 8J). Of note, centronuclear orange staining indicative of prophase/metaphase and speckled nuclear staining indicative of anaphase were observed with this mitotic marker. In contrast, 5.9% ± 0.1% of ventricular cardiomyocytes expressed pHH3 in *Myocd*$^{-/-}$ hearts (Figure 8K) ($P < 0.001$ versus WT hearts). However, when grown in the presence of BMP10-conditioned medium, 13.6% ± 0.1% of *Myocd*$^{-/-}$ ventricular cardiomyocytes were pHH3 positive (Figure 8L) ($P < 0.01$ versus control medium). Moreover, consistent with the changes observed in vivo, 7.9% ± 0.7% of cardiomyocytes in control hearts expressed the cell cycle inhibitor p57^{kip2} (Figure 8M), while 35.3% ± 0.9% of ventricular cardiomyocytes in *Myocd*$^{-/-}$ hearts expressed p57^{kip2} (Figure 8N). However, when grown in the presence of Bmp10-conditioned

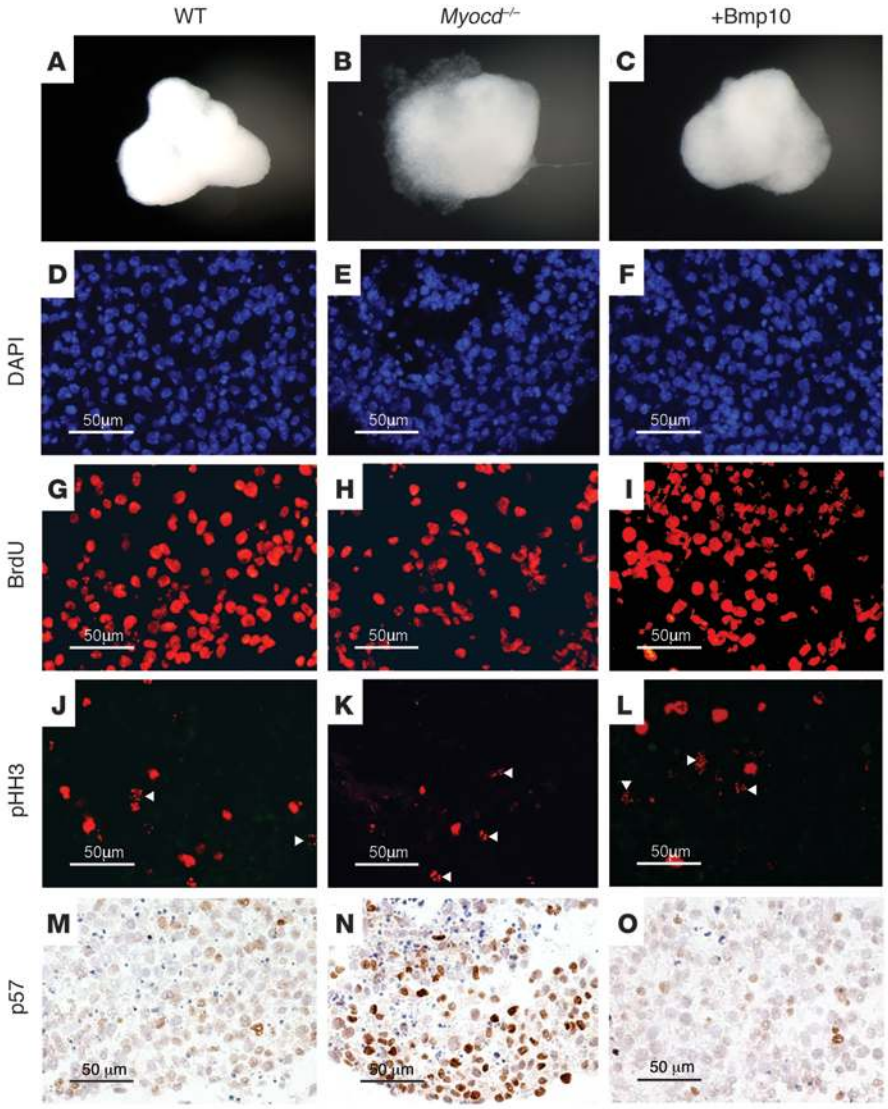

Figure 8

Bmp10 rescues the defect in cardiomyocyte proliferation and p57^{kip2} expression observed in *Myocd*$^{-/-}$ hearts. E9.5 WT and *Myocd*$^{-/-}$ mutant hearts were grown for 48 hours in conditioned medium harvested from NIH3T3 cells that were stably transduced with lentivirus encoding EGFP (control) or mouse Bmp10 (+ Bmp10) (n = 5 hearts per group). (**A**–**C**) Whole mount of WT heart (**A**), *Myocd*$^{-/-}$ heart grown in control medium (**B**), and *Myocd*$^{-/-}$ heart grown in Bmp10-conditioned medium (**C**). *Myocd*$^{-/-}$ hearts were smaller than WT hearts and beat more slowly and less vigorously. See also Supplemental Videos 7–10. (**D**–**F**) DAPI staining (blue nuclear stain) of WT, *Myocd*$^{-/-}$, and *Myocd*$^{-/-}$ + Bmp10 explanted hearts. Scale bars in microns are shown. (**G**–**I**) BrdU incorporation in WT, *Myocd*$^{-/-}$, and *Myocd*$^{-/-}$ explanted hearts grown in Bmp10-conditioned medium. Sections of explanted hearts were immunostained with BrdU antibody (orange stain). BrdU-positive cardiomyocytes per high power field were quantified by a blinded observer, and data are expressed as mean percentage of BrdU-positive cardiomyocytes ± SEM. (**J**–**L**) pHH3 expression (orange stain) in WT, *Myocd*$^{-/-}$, and *Myocd*$^{-/-}$ explanted hearts grown in Bmp10 conditioned medium. Cardiomyocytes undergoing mitosis in prophase/metaphase exhibited centronuclear staining, while cardiomyocytes in anaphase (arrowheads) exhibit speckled nuclear staining. pHH3-positive cardiomyocytes per high power field were quantified by a blinded observer and data expressed as mean percentage of pHH3-positive cardiomyocytes ± SEM. (**M**–**O**) Sections immunostained for p57^{kip2} (brown stain) demonstrating marked increased in p57^{kip2} in *Myocd*$^{-/-}$ heart, which decreases significantly when grown in Bmp10-conditioned medium.

medium, only 9.9% ± 0.8% of ventricular cardiomyocytes expressed p57^{kip2} (Figure 8O) (P < 0.001 versus control medium). In contrast, no significant difference was observed in apoptosis as detected by TUNEL staining between *Myocd*$^{-/-}$ hearts grown in control and Bmp10-conditioned medium (data not shown).

Discussion

The molecular programs regulating development and morphogenesis of the heart are dependent upon the capacity of cardiomyocytes to transduce and respond to developmental cues and environmental signals. Analyses of genetically engineered mice harboring null and conditional loss-of-function mutations in the *Myocd* gene have shown that myocardin plays a critical role in regulating vascular SMC differentiation and patterning of the vascular system (13, 14). However, despite the finding that myocardin is expressed early and abundantly in the embryonic heart, its role, if any, in promoting cardiomyocyte differentiation and cardiac morphogenesis has remained unclear. The data presented in this report demonstrate unequivocally that in the embryonic heart, myocardin is not required for cardiac myocyte specification and/or looping morphogenesis, but is required for cardiac growth and chamber maturation, maintenance of cardiac function, and ultimately, embryonic survival. Surprisingly, the basis of myocardin function is not predicted by its activity in vascular SMC differentiation, but rather via the capacity to regulate cardiomyocyte proliferation and apoptosis in the embryonic heart, acting at least in part via activation of the *Bmp10* gene.

As schematically shown in Figure 9, in the embryonic heart, myocardin is poised to respond to developmental cues, growth factors, and hemodynamic signals influencing the balance of cardiomyocyte proliferation and apoptosis required for atrial and ventricular chamber maturation. After completion of looping morphogenesis, coincident with the onset of rapid growth associated with chamber maturation, myocardin acting via induction of *Bmp10* gene expression represses activity of the cell cycle inhibitor p57^{kip2}, stimulating cardiomyocyte proliferation. During this developmental window, myocardin is also required for maintenance of a subset of key cardiogenic factors, including Nkx2-5 and Mef2c (20). BMP-induced activation of *Nkx2-5* gene transcription

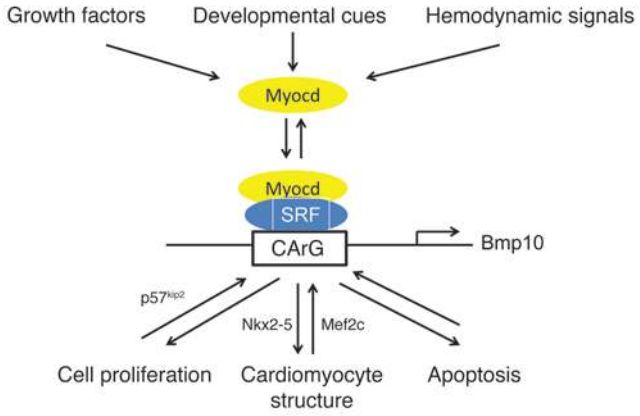

Figure 9
Myocardin transduces signals regulating Bmp10 signaling required for cardiac chamber maturation. In the schematic model, following cardiac looping at the onset of rapid heart cardiac growth associated with atrial and ventricular chamber maturation, myocardin transduces signals that promote binding of a myocardin-SRF protein complex to the nonconsensus CArG box regulating transcription of the *Bmp10* gene as well as other CArG boxes regulating transcription of a subset of cardiac-restricted genes. Bmp10, in turn, represses $p57^{kip2}$, promoting cardiomyocyte proliferation. In addition, Bmp10 is required for maintenance of a subset of key cardiogenic factors, including Nkx2-5 and Mef2c, that regulate structural organization of the cardiomyocyte. Finally, myocardin blocks programmed cell death in the cardiomyocyte, and myocardin deficiency is associated with a dramatic increase in cardiomyocyte apoptosis.

occurs via binding of Smad1/4 to the *Nkx2-5* transcriptional enhancer (32). Consistent with these observations, conditional ablation of the *Nkx2-5* gene at E12.5 leads to a block in chamber maturation, recapitulating the phenotype observed in *Myocd* conditional mutant embryos (33). Moreover, in the primitive heart, at least as early as E8.5, myocardin represses cardiomyocyte apoptosis, preserving cardiac function. Taken together, these data demonstrate that as a transcriptional coactivator, myocardin transduces signals influencing cardiomyocyte proliferation, structural organization of the cardiomyocyte, and programmed cell death required for the late stages of cardiac morphogenesis needed for atrial and ventricular chamber maturation.

The demonstration that cardiogenic factors including Nkx2-5 and Mef2c are downregulated in the hearts of E9.5 $Myocd^{-/-}$ embryos was initially perplexing because $Myocd^{-/-}$ embryos progress through the early stages of cardiogenesis, including formation of the primitive heart tube and looping morphogenesis, while $Nkx2\text{-}5^{-/-}$ and $Mef2c^{-/-}$ embryos exhibit a block in looping morphogenesis (25–27). What explains the divergent phenotype of $Myocd^{-/-}$ versus $Nkx2.5^{-/-}$ and $Mef2c^{-/-}$ mutant embryos? Surprisingly, at E8.0–E8.5, prior to initiation of cardiac looping, Nkx-2.5 and Mef2c are expressed at comparable levels in control and $Myocd^{-/-}$ embryos (Supplemental Figure 2). Similarly, comparable levels of Nkx-2.5 and Mef2c were observed at E8.5 in control and $Bmp10^{-/-}$ embryos (20). These data define a developmental window when myocardin (and Bmp10) regulates expression of the cardiogenic transcription factors Nkx-2-5 and Mef2c. This window occurs after formation of the primitive heart tube and looping morphogenesis (E8.0–E8.5 in the mouse) coincident with chamber maturation of the embryonic heart (E9.5). This observation highlights the role of myocardin as a transcriptional coactivator that is capable of transducing and responding to specific developmental cues in the embryonic heart.

Surprisingly, some, but not all, of myocardin-regulated functions in the embryonic heart are conserved in the heart during postnatal development. *Myocd* gene ablation in the adult heart is accompanied by dissolution of sarcomeric organization, disruption of the intercalated disc, and cell-autonomous loss of cardiomyocytes via apoptosis (16). The structural defects are attributable, at least in part, to a block in SRF-dependent genes encoding a subset of myofibrillar and structural proteins, including α-cardiac actin, MLC2v, desmin, and connexin 43 (16). Interestingly, each of these proteins is observed in the hearts of E9.5 $Myocd^{-/-}$ embryos (J. Huang, unpublished observations), suggesting that MRTF-A/MKL1 and/or MRTF-B/MKL2 may subserve a partially redundant function with myocardin in the embryonic heart: a capacity that is lost during postnatal development. In this regard, it is noteworthy that the structure of the sarcomere and the repertoire of genes encoding myofibrillar proteins are distinct in the embryonic and adult heart. In contrast, throughout development, myocardin represses programmed cell death in the cardiomyocyte.

The molecular basis of myocardin function in the embryonic heart was not anticipated by a decade of studies that defined its functions in SMCs and the vasculature (13, 14). Ectopic expression of myocardin in *X. laevis* embryos activates some, but not all, SRF-regulated genes encoding contractile proteins expressed in the fetal heart (15). The fetal heart program includes the transient expression of a select group of SRF-regulated genes encoding SMC-restricted contractile proteins, including SMA and SM22α, which are transiently expressed in the embryonic heart and reexpressed in the adult heart in response to hemodynamic stress. At E9.5, SM22α and SMA are not expressed in vascular SMCs populating the dorsal aorta of $Myocd^{-/-}$ embryos (13). This led us to postulate that the defects observed in the hearts of $Myocd^{-/-}$ embryos were caused, at least in part, by a block in expression of the subset of SRF-dependent genes encoding SMC-restricted contractile proteins. Interestingly, this is not the case, as comparable levels of SM22α and SMA were observed in the hearts of $Myocd^{-/-}$ embryos and control littermates. Taken together, these data demonstrate that distinct transcriptional mechanisms have evolved to control the expression of SRF-dependent genes encoding SMC contractile proteins in the embryonic heart and vasculature, respectively.

For many years it has been recognized that a subset of BMP growth factors plays critical roles in the morphogenetic program regulating development of the heart (17, 18). However, the mechanisms regulating expression of BMPs in the heart remain poorly understood. The findings that (a) *Bmp10* gene expression is markedly downregulated in the hearts of $Myocd^{-/-}$ and cardiomyocyte-restricted conditional mutant embryos, (b) forced expression of myocardin transactivates the *Bmp10* promoter via binding of a myocardin/SRF protein complex to a conserved CArG box, (c) expression of phosphorylated Smad1/5/8 is repressed in $Myocd^{-/-}$ hearts at E9.5, (d) Bmp10-regulated genes including Nkx2-5 and Mef2c are suppressed in the hearts of $Myocd^{-/-}$ and $Bmp10^{-/-}$ embryos, (e) $p57^{kip2}$ is induced in the hearts of $Myocd^{-/-}$ and $Bmp10^{-/-}$ embryos, (f) Bmp10-conditioned medium rescues the proliferative

defect in *Myocd*$^{-/-}$ mutant hearts and suppresses p57^{kip2}, and most importantly, (g) shared morphogenetic defects are observed in the hearts of *Myocd*$^{-/-}$, *Nkx2-5Cre*$^{+}$*Myocd*$^{F/F}$, and *Bmp10*$^{-/-}$ embryos strongly support the conclusion that myocardin (and SRF) regulates transcription of the *Bmp10* gene in the embryonic heart. This conclusion was not anticipated by a decade of research into the function of myocardin, which had not suggested a role for myocardin in the regulation of BMP-related growth factors.

The demonstration of apoptosis in the hearts of *Myocd*$^{-/-}$ and *Nkx2-5Cre*$^{+}$*Myocd*$^{F/F}$ mutant embryos reveals a conserved function for myocardin throughout development of the heart. Consistent with this observation, conditional ablation of *Srf* in the embryonic heart is associated with increased cardiomyocyte apoptosis and heart failure (8). In this regard, it is noteworthy that Bmp10 did not rescue apoptosis in *Myocd*$^{-/-}$ mutant hearts, suggesting strongly that myocardin-induced repression of programmed cell death is not linked to cell proliferation and is independent of BMP10 signaling. This primal function of myocardin (and SRF) appears to be cell autonomous and not dependent upon hemodynamic signals because the loss of myocardin in primary neonatal cardiomyocytes in cell culture rapidly induces apoptosis, acting via the intrinsic and extrinsic apoptotic pathways (16). This observation raises a fundamental question: what is the evolutionary advantage of a transcriptional coactivator required for cardiomyocyte survival? Are there circumstances in the embryonic heart and/or when the heart adapts to hemodynamic stress in which cardiomyocyte apoptosis is beneficial? Does myocardin play a unique role in the embryonic heart in response to hemodynamic stress? The answers to these questions will provide new insights into understanding the molecular basis of cardiac morphogenesis and may be relevant to understanding the pathogenesis of heart failure and cardiomyopathy.

Methods

Generation of myocardin-null and conditional mutant mice. To generate *Myocd*$^{+/-}$ mutant mice, homozygous myocardin conditional mutant mice (*Myocd*$^{F/F}$) (16) were intercrossed with CMV-Cre (BALB/c-Tg(CMV-cre)1Cgn/J) transgenic mice (34). Southern blot analyses confirmed that the *Myocd* targeted allele was deleted and passed on through the germline (Supplemental Figure 1). Deletion of *Myocd* exon 8 creates an out-of-frame mutation and N-terminal truncation of the myocardin protein, which is effectively null (16). To delete *Myocd* selectively in embryonic cardiomyocytes, *Myocd*$^{F/F}$ mice were interbred with *Nkx2-5Cre* transgenic mice (24).

Histology and immunohistochemistry. Immunohistochemistry analyses were performed with the protocols reported previously (14). Antibodies utilized for immunohistochemistry studies are included in Supplemental Table 1. Quantification of apoptosis in the embryonic heart was assessed by TUNEL staining, as described previously (16). Histological sections were counterstained with MF20 antibody (Hybridoma Bank, University of Iowa, Iowa City, Iowa, USA) to identify cardiomyocytes.

EM and 3D optical mapping. EM and scanning EM studies were performed as described previously (14). Whole-mount immunostaining was performed with monoclonal anti-MLC2v primary antibody (AXXORA) and HRP-conjugated IgG secondary antibody (Cell Signaling), as described (35). High-resolution optical mapping studies were performed on an Olympus BX51WI microscope equipped with a high-speed CMOS camera (MiCAM ULTIMA L; SciMedia Ltd.), as described (36).

Echocardiography. Cardiac morphometric and echocardiographic measurements were performed as described previously (16). To measure systolic to diastolic ventricular dimension and calculate fractional shortening in E9.5 embryos, the outer edge of the common ventricle was traced during diastole and systole. The fraction shortening (%) was defined as (diastolic area – systolic area)/diastolic area.

qPCR, real-time qRT-PCR. DNA was isolated from the yolk sac of embryos or tail biopsies of weaned mice and genotype determined by PCR, as described previously (14). Real-time qRT-PCR was performed using the DNA Engine Opticon 2 Real Time Detection System (Applied Biosystems), as described previously (14). Expression of myocardin, *Srf*, *Nkx-2.5*, *Mef2c*, *Mkl1*, *Mkl2*, *Tbx5*, *Gata4*, *Mlc2v*, β-*myosin heavy chain*, *Bmp10*, and GAPDH genes was assessed with complementary primer pairs as described (14).

Cell culture, plasmid DNA preparation, and luciferase reporter assays. A search for conserved CArG motifs in *Bmp10* promoter across species was performed by searching GenBank using the TRASFAC database with the identify threshold set to greater than 85%. Transient cotransfection analyses of C3H10T1/2 and Cos7 cells were performed as described previously (37). The pcDNA3.1-MyocdL expression plasmid encodes the 935–amino acid mouse myocardin protein, and the pcDNA3.1-MyocdS expression plasmid encodes the 856–amino acid mouse myocardin protein isoform; these were reported previously (14). Mammalian expression plasmids encoding mouse myocardin and SRF were generated in pcDNA3 as described (14). The 795-bp mouse *Bmp10* promoter was generated via PCR and subcloned into SmaI/BglII-digested pGL3-Basic (Promega) luciferase reporter vector generating the pBmp10.luc reporter plasmid. The pμBmp10.luc promoter is identical to pBmp10.luc, but contains a 2-bp mutation in the mouse Bmp10 CArG box (CC to GG), which was generated using the QuikChange Site-Directed Mutagenesis kit (Stratagene). Transient cotransfections were performed using FuGENE 6 (Roche Applied Science), as described previously (14). Transcriptional activity was quantified by measuring firefly luciferase activity relative to the internal control TK-*Renilla* luciferase activity using the Dual Luciferase Assay System (Promega), as described (14). A minimum of 6 independent transfections were performed, and all assays were performed in triplicate. Results are reported as the relative luciferase activity ± SEM.

Quantitative ChIP assays. ChIP assays were performed using reagents and protocols from Upstate Biotechnology. Hearts harvested from E9.5 WT mouse embryos were homogenized and fixed with formaldehyde to crosslink chromatin. The crosslinked chromatin was immunoprecipitated with either an anti-SRF antibody (G20X; Santa Cruz Biotechnology), polyclonal anti-myocardin antibody (37), or preimmune rabbit sera (negative control). PCR primers to quantify enrichment of input DNA included the following: *c-fos* CArG: 5′-CGGTTCCCCCCCTGCGCTGCACCCTCAGAG-3′; 5′-AGAACAACAGGGACCGGCCGTGGAAACCTG-3′; *Bmp10* CArG: 5′-ATGACCGTGACATTCATTCTTTCCTG-3′; 5′-TTTGCACGTGTGTATGACAGATGTTAAG-3′. Data are expressed as fold enrichment (arbitrary units) normalized to input DNA ± SEM.

Immunoblot analyses. Western blot analyses were performed as described previously (14). The hybridization signal was quantified using Image Quant 5.0 software, as described by the manufacturer (Molecular Dynamics Inc.).

EMSAs. Nuclear protein extracts were prepared using NE-PER Nuclear and Cytoplasmic Extraction Reagents (Thermo Scientific). Binding reactions were performed using the Light Shift Chemiluminescent EMSA Kit (Thermo Scientific) according to the manufacturer's protocol. Biotin-labeled primers included the following: mouse Bmp10 CArG 5′-TTTATGCCATCTTTGGACATGT-3′; mouse *Bmp10* mut-CArG 5′-TTTATGGGATCTTTGGACATGT-3′; human *BMP10* CArG 5′-GTCTTTCCTAATCTGGACACAA-3′; human *BMP10* CArG 5′-TTGTGTCCAGATTAGGAAAGAC-3′.

Generation of Bmp10-conditioned medium and ex vivo culture of embryonic hearts. The mouse Bmp10 cDNA was generated via PCR and subcloned into the pSMPUW-IRES-GFP lentiviral expression vector. HEK293T cells

were transfected for Bmp10 lentiviral expression and EGFP control virus production and purification according to the manufacturer's instructions (Cell Biolabs). NIH3T3 cells were transduced with lentiviral supernatants and cultured for 2 days in DMEM containing 10% FBS as described (20). Embryonic hearts were dissected from E9.5 embryos and cultured ex vivo for 48 hours as described (20). At 24 hours after isolation, BrdU was added to the control or Bmp10 conditioned medium and hearts were harvested 24 hours later for histological analyses.

Statistics. All measurement data are expressed as mean ± SEM. The statistical significance of differences between groups was determined by 2-tailed Student's *t* test. Differences were considered significant at a *P* value of less than 0.05.

Study approval. All animal experimentation was performed under protocols approved by the University of Pennsylvania IACUC and in accordance with NIH guidelines.

Acknowledgments

We thank Jon Epstein, Mark Kahn, and Ed Morrisey for their advice and helpful comments. We thank Kurt Engleka for assistance with 3D optical mapping. This work was supported in part by NIH R01-HL102968 and R01-HL094520 and the Commonwealth of Pennsylvania.

Received for publication February 28, 2012, and accepted in revised form July 26, 2012.

Address correspondence to: Michael S. Parmacek, University of Pennsylvania Cardiovascular Institute, 11-122 Translational Research Center, 3400 Civic Center Blvd., Bldg. 421, Philadelphia, Pennsylvania 19104-5159, USA. Phone: 215.746.4635; Fax: 215.349.8017; E-mail: Michael.parmacek@uphs.upenn.edu.

1. Olson EN. A genetic blueprint for growth and development of the heart. *Harvey Lect*. 2002;98:41–64.
2. Srivastava D, Olson EN. A genetic blueprint for cardiac development. *Nature*. 2000;407(6801):221–226.
3. Wolf M, Basson CT. The molecular genetics of congenital heart disease: a review of recent developments. *Curr Opin Cardiol*. 2010;25(3):192–197.
4. Moon A. Mouse models of congenital cardiovascular disease. *Curr Top Dev Biol*. 2008;84:171–248.
5. Olson EN. Development. The path to the heart and the road not taken. *Science*. 2001; 291(5512):2327–2328.
6. Olson EN, Schneider MD. Sizing up the heart: development redux in disease. *Genes Dev*. 2003; 17(16):1937–1956.
7. Barron MR, et al. Serum response factor, an enriched cardiac mesoderm obligatory factor, is a downstream gene target for Tbx genes. *J Biol Chem*. 2005; 280(12):11816–11828.
8. Niu Z, et al. Conditional mutagenesis of the murine serum response factor gene blocks cardiogenesis and the transcription of downstream gene targets. *J Biol Chem*. 2005;280(37):32531–32538.
9. Balza RO, JrMisra RP. Role of the serum response factor in regulating contractile apparatus gene expression and sarcomeric integrity in cardiomyocytes. *J Biol Chem*. 2006;281(10):6498–6510.
10. Miano JM, et al. Restricted inactivation of serum response factor to the cardiovascular system. *Proc Natl Acad Sci U S A*. 2004;101(49):17132–17137.
11. Parmacek MS. Myocardin-related transcription factors: critical coactivators regulating cardiovascular development and adaptation. *Circ Res*. 2007; 100(5):633–644.
12. Wang D, et al. Activation of cardiac gene expression by myocardin, a transcriptional cofactor for serum response factor. *Cell*. 2001;105(7):851–862.
13. Li S, Wang DZ, Wang Z, Richardson JA, Olson EN. The serum response factor coactivator myocardin is required for vascular smooth muscle development. *Proc Natl Acad Sci U S A*. 2003;100(16):9366–9370.
14. Huang J, et al. Myocardin regulates expression of contractile genes in smooth muscle cells and is required for closure of the ductus arteriosus in mice. *J Clin Invest*. 2008;118(2):515–525.
15. Small EM, Warkman AS, Wang DZ, Sutherland LB, Olson EN, Krieg PA. Myocardin is sufficient and necessary for cardiac gene expression in Xenopus. *Development*. 2005;132(5):987–997.
16. Huang J, et al. Myocardin is required for cardiomyocyte survival and maintenance of heart function. *Proc Natl Acad Sci U S A*. 2009;106(44):18734–18739.
17. Schneider MD, Gaussin V, Lyons KM. Tempting fate: BMP signals for cardiac morphogenesis. *Cytokine Growth Factor Rev*. 2003;14(1):1–4.
18. Nakajima Y, Yamagishi T, Hokari S, Nakamura H. Mechanisms involved in valvuloseptal endocardial cushion formation in early cardiogenesis: roles of transforming growth factor (TGF)-beta and bone morphogenetic protein (BMP). *Anat Rec*. 2000; 258(2):119–127.
19. Neuhaus H, Rosen V, Thies RS. Heart specific expression of mouse BMP-10 a novel member of the TGF-beta superfamily. *Mech Dev*. 1999;80(2):181–184.
20. Chen H, et al. BMP10 is essential for maintaining cardiac growth during murine cardiogenesis. *Development*. 2004;131(9):2219–2231.
21. Chen H, et al. Overexpression of bone morphogenetic protein 10 in myocardium disrupts cardiac postnatal hypertrophic growth. *J Biol Chem*. 2006; 281(37):27481–27491.
22. Nakano N, et al. Interaction of BMP10 with Tcap may modulate the course of hypertensive cardiac hypertrophy. *Am J Physiol Heart Circ Physiol*. 2007; 293(6):H3396–H3403.
23. Owens GK. Molecular control of vascular smooth muscle cell differentiation. *Acta Physiol Scand*. 1998; 164(4):623–635.
24. Moses KA, DeMayo F, Braun RM, Reecy JL, Schwartz RJ. Embryonic expression of an Nkx2-5/Cre gene using ROSA26 reporter mice. *Genesis*. 2001; 31(4):176–180.
25. Lyons I, et al. Myogenic and morphogenetic defects in the heart tubes of murine embryos lacking the homeo box gene Nkx2-5. *Genes Dev*. 1995;9(13):1654–1666.
26. Tanaka M, Chen Z, Bartunkova S, Yamasaki N, Izumo S. The cardiac homeobox gene Csx/Nkx2.5 lies genetically upstream of multiple genes essential for heart development. *Development*. 1999; 126(6):1269–1280.
27. Lin Q, Schwarz J, Bucana C, Olson EN. Control of mouse cardiac morphogenesis and myogenesis by transcription factor MEF2C. *Science*. 1997; 276(5317):1404–1407.
28. Ip HS, et al. The GATA-4 transcription factor transactivates the cardiac muscle-specific troponin C promoter-enhancer in nonmuscle cells. *Mol Cell Biol*. 1994;14(11):7517–7526.
29. Owens GK, Kumar MS, Wamhoff BR. Molecular regulation of vascular smooth muscle cell differentiation in development and disease. *Physiol Rev*. 2004;84(3):767–801.
30. Eivers E, Demagny H, De Robertis EM. Integration of BMP and Wnt signaling via vertebrate Smad1/5/8 and Drosophila Mad. *Cytokine Growth Factor Rev*. 2009;20(5–6):357–365.
31. Creemers EE, Sutherland LB, McAnally J, Richardson JA, Olson EN. Myocardin is a direct transcriptional target of Mef2, Tead and Foxo proteins during cardiovascular development. *Development*. 2006;133(21):4245–4256.
32. Brown CO 3rd, Chi X, Garcia-Gras E, Shirai M, Feng XH, Schwartz RJ. The cardiac determination factor, Nkx2-5, is activated by mutual cofactors GATA-4 and Smad1/4 via a novel upstream enhancer. *J Biol Chem*. 2004;279(11):10659–10669.
33. Terada R, Warren S, Lu JT, Chien KR, Wessels A, Kasahara H. Ablation of Nkx2-5 at mid-embryonic stage results in premature lethality and cardiac malformation. *Cardiovasc Res*. 2011;91(2):289–299.
34. Schwenk F, Baron U, Rajewsky K. A cre-transgenic mouse strain for the ubiquitous deletion of loxP-flanked gene segments including deletion in germ cells. *Nucleic Acids Res*. 1995;23(24):5080–5081.
35. Takakura N, Yoshida H, Ogura Y, Kataoka H, Nishikawa S. PDGFR alpha expression during mouse embryogenesis: immunolocalization analyzed by whole-mount immunohistostaining using the monoclonal anti-mouse PDGFR alpha antibody APA5. *J Histochem Cytochem*. 1997;45(6):883–893.
36. Rentschler S, et al. Notch signaling regulates murine atrioventricular conduction and the formation of accessory pathways. *J Clin Invest*. 2011; 121(2):525–533.
37. Du KL, et al. Myocardin is a critical serum response factor cofactor in the transcriptional program regulating smooth muscle cell differentiation. *Mol Cell Biol*. 2003;23(7):2425–2437.